Doping of Ga_2O_3 bulk crystals and NWs by ion implantation

K. Lorenz[*a,b], M. Peres[a], M. Felizardo[a], J. G. Correia[a], L.C. Alves[a], E. Alves[a,b], I. López[c], E. Nogales[c], B. Méndez[c], J. Piqueras[c], M. B. Barbosa[d], J. P. Araújo[d], J. N. Gonçalves[e], J. Rodrigues[f], L. Rino[f], T. Monteiro[f], E. G. Víllora[g], K. Shimamura[g]

[a]Instituto Superior Técnico (IST), Campus Tecnológico e Nuclear, Estrada Nacional 10, P-2695-066 Bobadela LRS, Portugal; [b]IPFN, IST, Portugal; [c]Dpto. Física de Materiales, Universidad Complutense de Madrid, 28040 Madrid, Spain; [d]IFIMUP and IN - Institute of Nanoscience and Nanotechnology, Departamento de Física e Astronomia da Faculdade de Ciências da Universidade do Porto, 4169-007 Porto, Portugal; [e]Departamento de Física e CICECO, Universidade de Aveiro, 3810-193 Portugal, [f]Departamento de Física e i3N, Universidade de Aveiro, 3810-193 Portugal; [g]National Institute for Materials Science, 1-1 Namiki, Tsukuba 305-0044, Japan

ABSTRACT

Ga_2O_3 bulk single crystals have been implanted with 300 keV Europium ions to fluences ranging from 1×10^{13} to 4×10^{15} at/cm^2. The damage build-up and Eu-incorporation was assessed by Rutherford Backscattering Spectrometry in the channeling mode (RBS/C). RBS/C results suggest that implantation causes a mixture of defect clusters and extended defects such as dislocations. Amorphisation starts at the surface for fluences around 1×10^{15} at/cm^2 and then proceeds to deeper regions of the sample with increasing fluence. Amorphous regions and defect clusters are efficiently removed during rapid thermal annealing at ~1100 ºC; however, Eu diffuses towards the surface. Nevertheless, Eu ions are optically activated and show cathodoluminescence at room temperature. Results in bulk samples are compared to those in Eu-implanted Ga_2O_3 nanowires and despite strong similarities in the structural properties differences were found in the optical activation. Furthermore, damage and dopant incorporation studies were performed using the Perturbed Angular Correlation technique, which allows probing the immediate lattice surroundings of an implanted radioactive probe at the atomic level.

Keywords: Ga_2O_3, rare earth, ion implantation, Rutherford Backscattering Spectrometry (RBS), channeling, cathodoluminescence (CL) , photoluminescence (PL), Perturbed Angular Correlation

1. INTRODUCTION

Ga_2O_3, with its wide band gap of 4.8 eV, is a promising material for photonic devices working in the visible and ultraviolet spectral region, as transparent conductive oxide as well as for gas sensing, among many other applications[1,2,3]. Doping Ga_2O_3 with optically active rare earth (RE) ions may extend these functionalities taking advantage of the sharp and mostly temperature stable RE emission lines, which span a wide spectral range from the infrared to the ultraviolet. In particular, Eu-doping has been studied with view to its application in phosphors due to the intense red intra-4f^6 transitions of the Eu^{3+} ions[4]. In these studies Eu was successfully incorporated and optically activated in polycrystalline thin films[5], nanopowders[6] or nanowires (NWs)[7]. REs incorporation into single crystals, in contrast, remains challenging due their low solubility in the crystalline matrix. Incorporation of appreciable amounts of RE ions often leads to polycrystalline growth or even phase separation[8]. Ion implantation presents itself as a powerful technique to incorporate dopants in a reproducible way, with the possibility of easy lateral patterning and is less affected by solubility limits. It has been successfully used for RE doping of wide bandgap semiconductors such as GaN[9] and AlN[10]. In Ga_2O_3, ion implantation has recently been used for electrical doping with Si[11] and it has been previously applied by the present authors for the doping and optical functionalization of Ga_2O_3 NWs with Er, Eu and Gd ions[12,13,14].

In this work, Ga_2O_3 single crystals were implanted with Eu ions and compared to Ga_2O_3 NWs implanted in similar conditions[14]. In bulk Ga_2O_3 the implantation damage formation and its removal by rapid thermal annealing (RTA) was studied by Rutherford Backscattering Spectrometry and channeling (RBS/C). Implantation damage is efficiently

* lorenz@ctn.ist.utl.pt; phone (+351) 219 946 052; fax (+351) 219 946 285

Oxide-based Materials and Devices V, edited by Ferechteh H. Teherani, David C. Look, David J. Rogers, Proc. of SPIE Vol. 8987, 89870M · © 2014 SPIE
CCC code: 0277-786X/14/$18 · doi: 10.1117/12.2037627

Downloaded From: http://proceedings.spiedigitallibrary.org/ on 03/09/2014 Terms of Use: http://spiedl.org/terms

removed after RTA at 1100 ºC. Although Eu is not incorporated in substitutional lattice sites and diffuses towards the surface for annealing at 1100 ºC, optical activation of Eu^{3+} is achieved. The amorphisation and annealing behavior is found to be similar in bulk crystals and NWs. The incorporation of Eu in optically active sites, on the other hand, is promoted in NWs. Low fluence implantation of Cd, led to the incorporation of Cd into substitutional octahedral Ga-sites in both bulk crystals and NWs.

2. EXPERIMENTAL DETAILS

β-Ga_2O_3 bulk single crystals were grown using the floating zone technique in a set-up equipped with four halogen lamps and the corresponding ellipsoidal mirrors. Growth details have been reported previously[15]. The crystals were cleaved on the (1 0 0) plane, and subsequently cut into ~5×5 mm^2 samples. 300 keV Europium implantation has been performed at room temperature (RT), along the surface normal, to fluences from 1×10^{13} at/cm^2 to 4×10^{15} at/cm^2. β-Ga_2O_3 NWs have been synthesized by a thermal evaporation method from a metallic gallium source on a Ga_2O_3 pellet that behaved as substrate. Afterwards, they were deposited on silicon substrates and then implanted with 150 keV Eu ions to a fluence of 5×10^{15} at/cm^2.[14] Post-implant rapid thermal annealing (RTA) was performed for 30 s in an ANNEALSYS halogen lamp rapid thermal processor in flowing Argon gas at temperatures from 500 to 1200 ºC.

RBS/C was performed using a 2 MeV He^+ beam and a PIN diode detector at 160º backscattering angle as well as a Si surface barrier detector at 140º. Random spectra were analyzed using the NDF code to extract the Eu profile[16]. Aligned spectra were taken along the <201> direction, normal to the surface, and treated using the DECO code[17] which is based on the two-beam approximation[18] to take into account dechanneling and correctly extract defect profiles from RBS/C data.

The optical properties of the samples were assessed by RT cathodoluminescence (CL) spectroscopy in a Hitachi S2500 scanning electron microscope (SEM) using acceleration voltages, V_{acc}, between 1 and 5 kV. Photoluminescence excitation (PLE) was performed using a Xe lamp as excitation source coupled to a monochromator. Additionally photoluminescence (PL) spectra were collected using a Surelite II/10 pulsed Nd:YAG laser (1064 nm, 10 Hz repetition rate) coupled to a fourth harmonic generator crystal (Surelite SLD-II and SLF) in order to achieve 266 nm pulsed excitation with a ~5 ns pulse width and 60 mJ of energy. Detection was performed by diffracting the collected emission in an ORIEL MS-125 monochromator, with a 400 gr/mm grating and acquired in an ANDOR iccd (model DH-520, P46 phosphor coated).

Perturbed Angular Correlation (PAC) were performed at ISOLDE/CERN using a BaF_2 6-detector PAC setup and the radioactive probe $^{111m}Cd/^{111}Cd$ which was implanted with a 30 keV energy beam to low fluences of ~5×10^{11} at/cm^2 at RT[19]. In the case of the bulk crystals, only four of the six detectors were used arranged in one plane at 90º to each other.

3. RESULTS AND DISCUSSION

3.1 Implantation damage formation and annealing in bulk Ga_2O_3 single crystals

Figure 1 presents the RBS/C random and <201> aligned spectra of bulk Ga_2O_3 samples implanted to different fluences. The minimum yield, χ_{min}, is defined as the ratio of the yield of the aligned spectrum to that of the random spectrum and is a measure of the crystal quality of a single crystal. The as-grown samples show χ_{min}~10%, determined in an energy window corresponding to a ~20 nm thick layer just below the surface, revealing a good crystal quality. This value is slightly higher than typical values for commercial bulk ZnO crystals or epitaxial layers (χ_{min}~4%) [20,21], but may be influenced by the rough as-cleaved, non-polished surface.

After implantation the backscattering yield strongly increases due to the implantation induced defects, even for the lowest fluence of 1×10^{13} at/cm^2 (Fig. 1a). In particular for the two lowest fluences (1×10^{13} at/cm^2 and 1×10^{14} at/cm^2), high dechanneling yields are observed in the Ga-signal corresponding to the deeper, unimplanted regions of the samples (below ~1450 keV), while direct backscattering from defects (appearing as a peak at energies > 1475 keV) is low.

Downloaded From: http://proceedings.spiedigitallibrary.org/ on 03/09/2014 Terms of Use: http://spiedl.org/terms

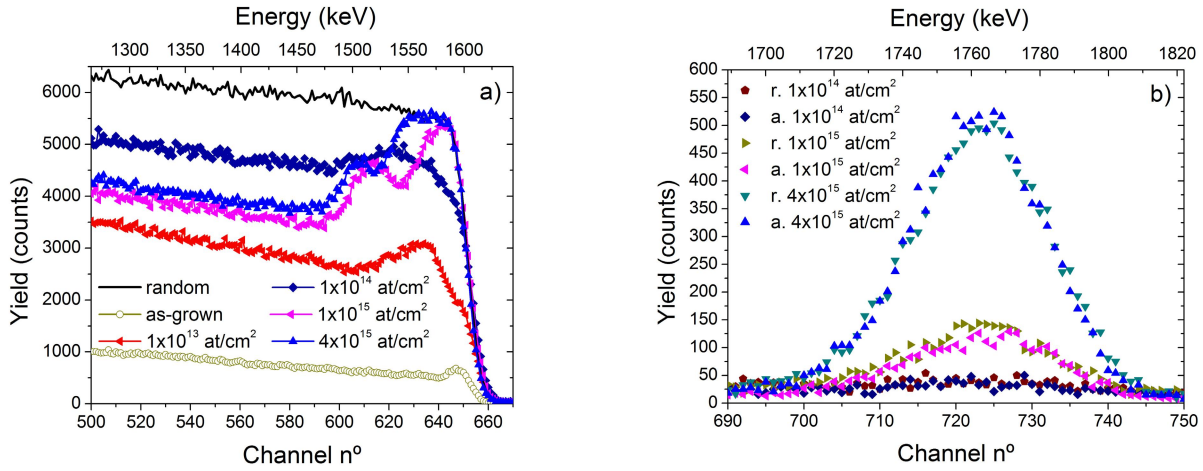

Figure 1. (a) Ga-signal of the RBS/C <201> aligned RBS/C spectra for the as-grown bulk Ga_2O_3 sample and after implantation of different Eu-fluences as well as a typical random spectrum. (b) Eu-signal of the random (r.) and <201> aligned (a.) RBS/C spectra for three different fluences.

High direct backscattering yields are usually ascribed to point defects, point defect clusters or amorphous zones with randomly displaced atoms. Extended defects, such as stacking faults or dislocation loops, on the other hand, lead to high dechanneling yields and low direct backscattering rates[22]. Therefore the high dechanneling yield observed for implanted Ga_2O_3 points to the formation of extended defects in the implanted zone. In agreement with this interpretation, the dechanneling yield decreases again for higher fluences when amorphisation sets in. Similar observations have been made in other wide bandgap semiconductors such as GaN and ZnO[20, 22].

For higher fluences a bimodal damage distribution is observed with a pronounced peak at the surface and a second peak deeper in the crystal. The surface peak is reaching the backscattering yield of the random level for a fluence of 1×10^{15} at/cm^2, which is commonly attributed to amorphisation (note, however, that RBS/C cannot distinguish between amorphous or polycrystalline material). Therefore, amorphisation in Ga_2O_3 is seen to start at the surface and then extends to deeper regions of the crystal with increasing fluence. This pronounced surface damage is unusual since the maximum nuclear energy deposition, which is assumed to be the main source for implantation damage in the present energy regime, has its maximum deeper inside the sample (at ~34 nm depth according to SRIM2013[23] Monte Carlo simulations). Very similar behavior has been found for ion implantation in GaN and its origin is still under debate[24,25,26].

In order to take into account the dechanneling yield and extract the defect profiles from the RBS/C data, the two-beam approximation was applied[18]; the resultant defect profiles are shown in Fig. 2. The two-beam approximation assumes two groups of ions, the "random beam", which is backscattered from both regular and displaced atoms and the "aligned beam", which is only backscattered from displaced atoms[27]. The probability for an ion to transit from the aligned to the random beam depends on the critical angle for dechanneling. The increased dechanneling yield in the presence of extended defects can then be introduced into the model by assuming a pre-factor to the critical angle. The validity of this approach is supported by the excellent agreement of the measured defect profile for the lowest fluence with the defect distribution calculated by the SRIM2013 code, which is also shown in Fig. 2. This result also confirms that the nuclear energy loss is responsible for the damage distribution for this low fluence.

For higher fluences, the defect profiles reach deeper into the crystal than predicted by SRIM simulations suggesting that now the Eu-impurity itself is involved in the damage build-up and/or defect diffusion becomes important. As mentioned before, for fluences $\geq 1\times10^{15}$ at/cm^2, the relative defect concentration at the surface reaches unity, which is a sign of amorphisation. For a fluence of 4×10^{15} at/cm^2, the amorphous layer increases and extends to a depth of ~70 nm.

Downloaded From: http://proceedings.spiedigitallibrary.org/ on 03/09/2014 Terms of Use: http://spiedl.org/terms

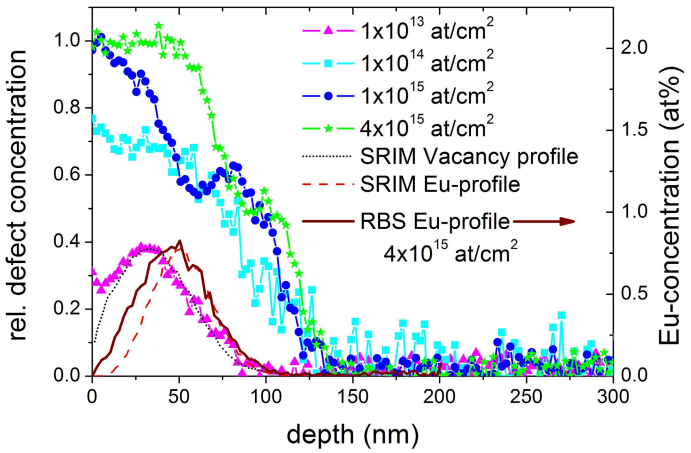

Figure 2. The relative defect concentration as a function of depth for bulk Ga_2O_3 crystals implanted to different Eu-fluences. The defect and Eu profiles calculated using the SRIM code are also shown (in arbitrary units) as well as the Eu-profile extracted from the RBS spectra of the sample implanted with 4×10^{15} at/cm^2.

The Eu-profiles as measured by RBS and calculated using SRIM2013 are also shown in Fig. 2. While the Eu-profiles agree well beyond a depth of ~50 nm, the measured Eu-profile starts at a shallower depth than expected from ballistic processes. A possible explanation is the diffusion of Eu during the implantation, which may be induced by the electronic energy deposited by the ion beam and facilitated by the implantation damage in the shallow regions of the sample. Beam heating should play a secondary role since annealing experiments do not show any diffusion for temperatures as high as 900 ºC (see below).

The sample implanted to the highest fluence was further subjected to an isochronous RTA treatment and RBS/C spectra were taken after each RTA step. The evolution of the defect and Eu distributions with annealing temperature is seen in Fig. 3. The defect concentration (see Fig. 3a) decreases only slightly after RTA at 500 ºC.

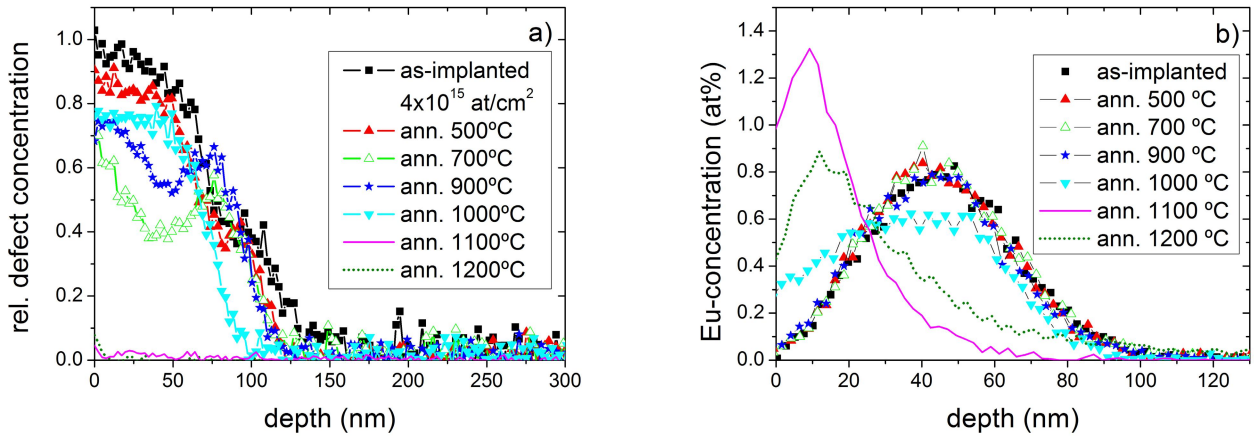

Figure 3. (a) The relative defect concentration as a function of depth of the Ga_2O_3 bulk sample implanted with 4×10^{15} at/cm^2 and subjected to isochronous annealing steps up to 1200 ºC and (b) the Eu-profiles after different RTA steps.

Downloaded From: http://proceedings.spiedigitallibrary.org/ on 03/09/2014 Terms of Use: http://spiedl.org/terms

After RTA at 700 ºC the defect concentration decreases strongly and the shape of the defect profile changes, showing two distinct peaks, one at the surface and another one beyond the maximum of the Eu-profile in the region which had not been amorphized in the as-implanted sample.

Surprisingly, the defect concentration is increasing for the next two annealing temperatures suggesting some defect rearrangement and clustering. This finding has been confirmed in a second sample implanted and annealed in the same conditions. Finally, for annealing at 1100 ºC the implantation damage is almost completely removed and at 1200 ºC the channeling quality of the as-grown sample is fully restored.

The Eu-profile does not change during RTA up to 900 ºC but Eu starts to diffuse towards the surface at 1000 ºC (Fig. 3b). After annealing at 1100 ºC Eu accumulates in a thin surface layer but no Eu is lost. At 1200 ºC, 5-10% of the Eu is lost while some Eu diffuses back into deeper layers of the crystal. Similar out-diffusion of implanted RE during post-implant annealing was also reported for ZnO[21] and is a sign of the low solubility of Eu in Ga_2O_3. Nevertheless, Eu is stabilized in a thin surface layer, possibly due to clustering with defects. In fact, random and aligned RBS/C spectra show an almost complete overlap of the Eu-signal for all fluences in the as-implanted (see Fig. 1b) as well as in the annealed samples (not shown) showing that the majority of Eu is incorporated in random positions in the Ga_2O_3 lattice.

3.2 Optical activation of Europium in bulk Ga_2O_3 single crystals

Fig. 4 shows RT CL spectra for the bulk samples implanted to 4×10^{15} at/cm^2 and annealed up to 1100 ºC. All samples, including the as-implanted one, exhibit the typical Eu^{3+} emission lines in the red spectral region around 600 nm as well as broad UV-blue emission bands centered at ~400-420 nm. The latter are typical for as-grown material[28]; however, the slight changes of their shape and position suggest that implantation defects and changes of the defect configuration during annealing also contribute to these bands. The relative intensity between the Eu^{3+} lines and the broad bands is strongly dependent on the excitation parameters, in particular, the excitation density. The spectra in Fig. 4 were normalized to the main Eu^{3+} emission peak at ~611 nm attributed to the $^5D_0\rightarrow{}^7F_2$ intraionic transition in agreement with previous reports in Eu-doped Ga_2O_3 films and nanostructures[4-8]. The annealing temperature has a strong effect on the Eu^{3+} lines as seen in Fig. 4b showing details of the $^5D_0\rightarrow{}^7F_J$ intraionic transitions.

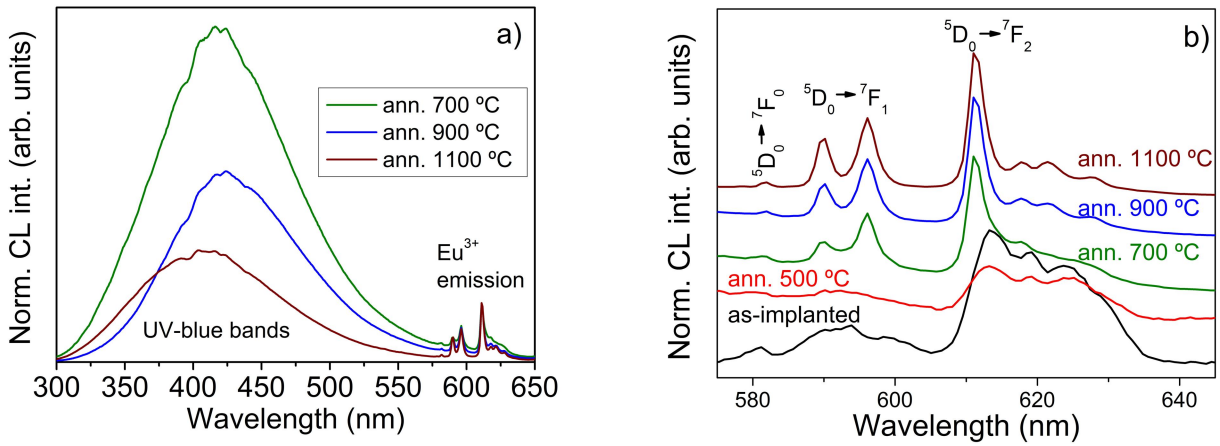

Figure 4. (a) RT CL spectra (V_{acc}=5 kV) of Ga_2O_3 bulk samples implanted with 4×10^{15} at/cm^2 and subjected to RTA up to 1100 ºC; the spectra were normalized to the main Eu^{3+} emission line at ~611 nm. (b) Normalized CL spectra, showing the wavelength region of the $^5D_0\rightarrow{}^7F_J$ intraionic Eu^{3+} transitions for different annealing temperatures.

Downloaded From: http://proceedings.spiedigitallibrary.org/ on 03/09/2014 Terms of Use: http://spiedl.org/terms

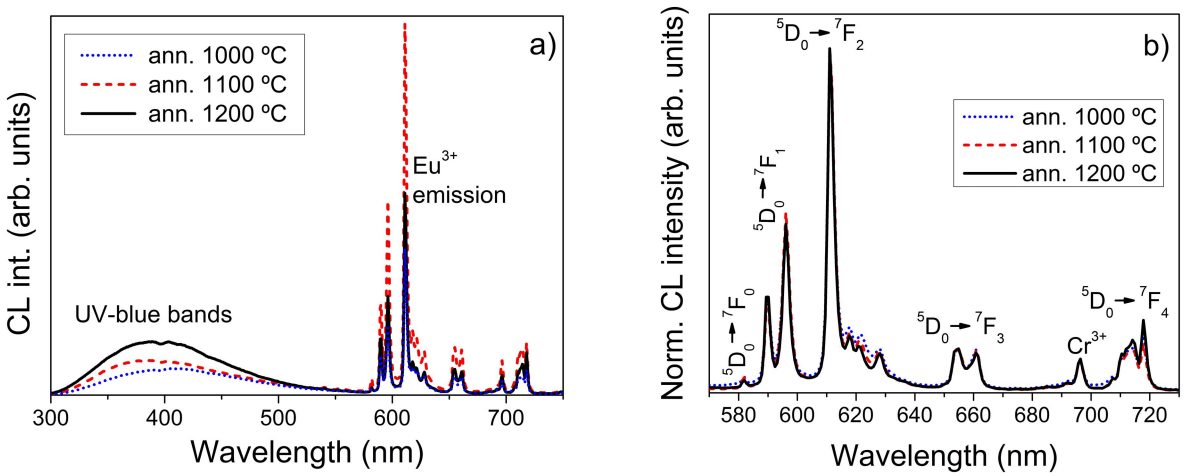

Figure 5. (a) RT CL spectra (V_{acc}=5 kV) of Ga_2O_3 bulk samples implanted with 4×10^{15} at/cm^2 and subjected to RTA up to 1200 ºC. (b) Normalized CL spectra, showing the wavelength region of the $^5D_0\rightarrow{}^7F_J$ intraionic Eu^{3+} transitions.

The Eu^{3+} lines are very broad in the as-implanted sample and that annealed at 500 ºC while they sharpen for higher annealing temperatures. This shows that the Eu-emission lines are very sensitive to disorder as already observed for Eu-implanted Ga_2O_3 NWs[14]. In fact, the strong line sharpening observed in the samples annealed at 700ºC and above are in good agreement with the improvement of their structural properties (section 3.1).

The good optical activation observed in the sample annealed at 1100 ºC is somewhat surprising having in mind the fact that at this temperature Eu diffuses towards the surface and occupies, in majority, random lattice sites. To study with more detail the effect of Eu diffusion towards the surface at high annealing temperatures, another sample set was prepared with annealing treatments at 1000, 1100, and 1200 ºC. The CL spectra, presented in Fig. 5, are dominated by the sharp $^5D_0\rightarrow{}^7F_J$ intraionic transition lines of Eu^{3+} (Fig. 5a) which are very sharp and well resolved (Fig. 5b). The Eu^{3+} emission intensity is seen to increase when increasing the annealing temperature from 1000 to 1100 ºC and then to slightly decrease after RTA at 1200 ºC.

Fig. 5b presents the normalized CL spectra in the red wavelength region of the $^5D_0\rightarrow{}^7F_J$ intraionic Eu^{3+} transitions. Besides the Eu^{3+} emission also the typical ~690 nm emission of Cr^{3+} is observed, which is a common unintentional impurity in Ga_2O_3[4]. The shape and relative line intensities nearly coincide for the different spectra indicating that no secondary phases are formed when Eu diffuses towards the surface and that the Eu centers are residing inside the Ga_2O_3 lattice.

Further CL measurements were carried out as a function of the electron beam acceleration voltage in order to get depth resolved information on the Eu^{3+} luminescence. The CL peak intensity ratios (normalized to the intensity of the sample annealed at 1000 ºC) are shown in Fig. 6 as a function of the acceleration voltage.

As shown in Ref. [13], the penetration depth of the electrons, as obtained by CASINO simulations, is in the range of 150 nm for 5 kV, 70 nm for 3 kV and 40 nm for 2 kV. For 1 kV the electrons penetrate down to about 15 nm. Therefore, from the RBS results we can say that for V_{acc} = 5 kV all the ions would be excited in the three samples. For 3 kV, still most of the ions are excited in the three samples. Finally, for 1 kV and 2 kV, the fraction of Eu residing in the volume of excitation is much higher in the 1100 and 1200ºC samples than in the 1000ºC sample.

The sample annealed at 1200 ºC shows 5-9 times higher CL intensity than the 1000 ºC-sample for low V_{acc}, i.e. the emission is coming from the surface-near region. This is in good agreement with the measured Eu-profile in this sample; however, the sample annealed at 1100 ºC does not show the same behavior although RBS also revealed an Eu-accumulation close to the surface in this sample. In fact, the CL intensity ratio between the 1100ºC and 1000ºC samples is seen to be relatively constant with increasing V_{acc}, indication that the distribution of luminescent Eu^{3+} centers is similar for both samples.

Downloaded From: http://proceedings.spiedigitallibrary.org/ on 03/09/2014 Terms of Use: http://spiedl.org/terms

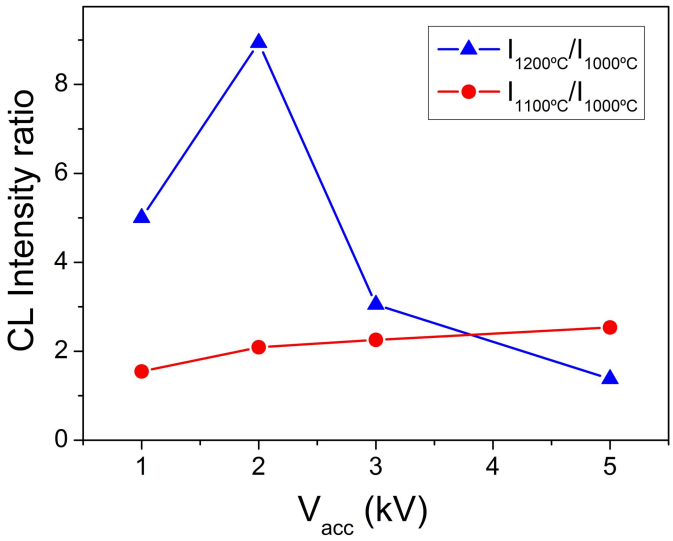

Figure 6. The CL intensity ratio of the Eu^{3+} emission lines of the Ga_2O_3 bulk samples implanted with 4×10^{15} at/cm^2 and annealed at different temperatures as a function of the e-beam acceleration voltage.

This discrepancy between CL and RBS, may be related with the fact that the majority of Eu atoms could not be incorporated in substitutional lattice sites. They may form clusters with other Eu atoms or with defects that lead to a quenching of the Eu^{3+} emission, which would also explain the incorporation into random lattice sites. The plot of the CL $I_{1100ºC}/I_{1000ºC}$ ratio with the acceleration voltage indicates that the optically active ions in 1000ºC and 1100ºC samples are not close to the surface in contrast to the 1200 ºC sample. Furthermore, the intensity of the 1100 ºC sample is about two times higher than that for the 1000 ºC sample revealing higher optical activation despite the Eu-diffusion.

3.3 Comparing the behavior of Eu in bulk Ga_2O_3 single crystals and nanowires

Compared to β-Ga_2O_3 NWs, which have been implanted in similar conditions as the single crystals in the present study[14], several similarities are found: 1. Both single crystals and NWs are amorphized for high fluence (4×10^{15} at/cm^2) Eu implantation. In the case of the NWs amorphization and crystal recovery during RTA were studied by Raman spectroscopy and transmission electron microscopy. (Note that RBS/C measurements are not possible in randomly oriented NWs since the 1 mm diameter beam is averaging over many NWs). 2. In both materials, partial damage removal is observed for RTA at 700 ºC and virtually complete lattice recovery is observed for annealing at 1100 ºC. 3. Similar CL spectral shapes suggest that the optically active Eu^{3+} centers are the same in both NWs and bulk Ga_2O_3. Furthermore, both materials show the same dependence of the Eu^{3+} emission line widths on the annealing temperature confirming the similarities in the mechanisms of defect formation and removal.

An important difference between Eu-implanted bulk crystals and NWs is their luminescence behavior upon photoexcitation. Fig. 7a shows a typical PLE spectrum of an Eu-implanted bulk crystal monitored at the broad blue emission peaked at 415 nm. Efficient excitation of this band is observed for wavelengths below ~275 nm, which is close to the Ga_2O_3 bandgap at ~258 nm. The PL spectrum for excitation at 266 nm, also shown in Fig. 7a, clearly reveals this broad band. However, the typical red Eu^{3+} emission is not observed in any of the bulk samples even when using a higher excitation density with the Nd:YAG laser, although it has been shown previously that Eu in Ga_2O_3 polycrystals can be excited by this wavelength[8].

Downloaded From: http://proceedings.spiedigitallibrary.org/ on 03/09/2014 Terms of Use: http://spiedl.org/terms

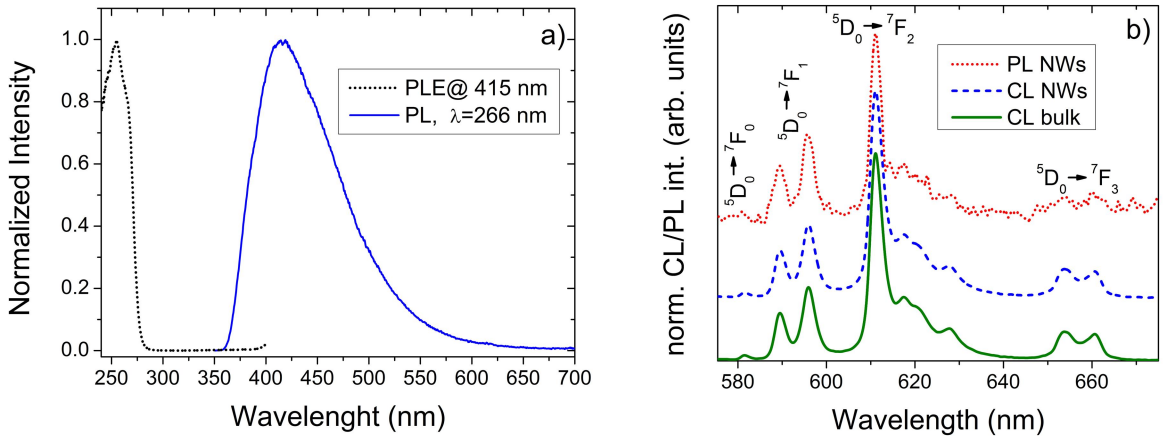

Figure 7. (a) RT PLE spectrum of an Eu-implanted bulk sample monitored at the peak of the blue band at 415 nm and the PL spectrum for lamp excitation at 266 nm. (b) Normalized PL (266 nm laser excitation) and CL spectra of the Eu-implanted and annealed NWs and bulk crystals at RT.

In contrast, Eu is efficiently excited by the 266 nm laser line in the implanted Ga_2O_3 NWs as seen in Fig. 7b, which is comparing the RT PL spectrum of an Eu-implanted and annealed NW sample with the CL spectra of the Eu-implanted and annealed NWs and the bulk crystal. The line shape of the three spectra is identical suggesting that the same Eu^{3+} centers are active in bulk crystals and NWs and that they can be efficiently excited by either electrons or laser light. It is interesting to note, that Eu^{3+} can be more easily excited in NWs than in bulk which may point to a better incorporation of Eu^{3+} in Ga-sites when implanted into NWs than when implanted into bulk crystals.

3.4 Lattice site location of implanted ^{111}Cd in Ga_2O_3 bulk single crystals and nanowires

Lattice site location measurements in NWs are challenging since routinely applied techniques such as RBS/C or emission channeling rely on macroscopic single crystalline host materials[29]. Synchrotron X-ray absorption near edge structure and extended X-ray absorption fine structure data have been used for lattice site location measurements in NWs[30]. In Ga_2O_3 NWs we applied the Perturbed Angular Correlation (PAC) technique to infer, particularly, on the lattice site of implanted radioactive ^{111m}Cd probes[19], being Cd in this case a conceptually interesting p-type dopant.

The PAC technique is used to characterize, at the nanoscopic scale, the local crystal field and point defects charge distribution at a selected probe atom. The technique applies radioactive nuclei with appropriate excited states, where their magnetic and quadrupole moments interact with the outer magnetic field (B) and / or electric field gradients (EFGs) from the host. The measurement relies on the hyperfine interaction of the EFG with the nuclear quadrupole moment of the intermediate state of a γ–γ cascade in the daughter nucleus[31,32]. The PAC experimental observable is the "anisotropy ratio" function R(t), a histogram build as a function of time between detection of γ1 and detection of γ2, during decay of about 10^{11} - 10^{12} atoms. The time-dependence of the R(t) function contains the information on the EFG. The latter is characterized by the quadrupole interaction frequency ν_Q and the axial asymmetry parameter η . ν_Q is proportional to the product of the EFG principal component, V_{zz}, with the quadrupole moment Q of the intermediate state of the cascade. In the case of ^{111m}Cd, the intermediate state has spin 5/2 that splits into three hyperfine energy levels, where each EFG - each different local electronic configuration- is characterized by three frequencies, which are visible in the R(t) and respective Fourier transform spectra, with their relative strengths depending on the measurement geometry of the single crystal. Each fraction of probe nuclei interacting with different EFGs will produce a different triplet with scaled and proportional intensities.

Downloaded From: http://proceedings.spiedigitallibrary.org/ on 03/09/2014 Terms of Use: http://spiedl.org/terms

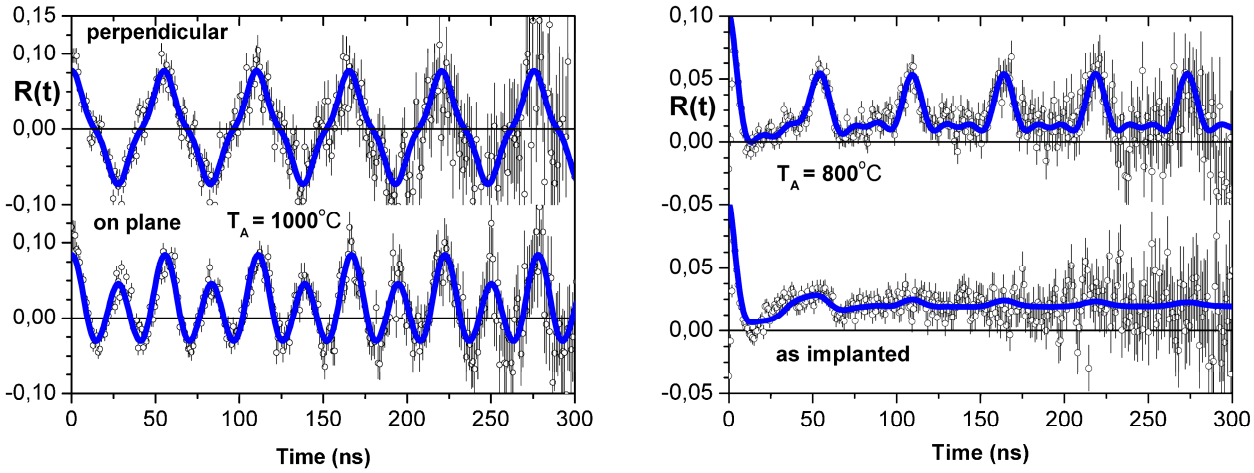

Figure 8. (a) RT PAC spectra of a ^{111m}Cd implanted bulk Ga_2O_3 crystal after annealing at 1000 ºC for 20 min in air. Spectra were taken in two different geometries: with the <201> axis perpendicular to the detector plane (top); and with the <201> axis lying in the detector plane, aligned with the angle bisector of two detectors at a relative angle of 45° between axis and detectors (bottom). (b) RT PAC spectra of the as-implanted NW sample and after annealing at 800 ºC (adapted from [19] with permission from WILEY).

In this way PAC is well suited to explore the lattice sites and next neighbor defects of certain radioactive probe elements at the atomic scale, in a wide variety of samples including bulk single crystals, powders, thin films and nanocrystals[19].

Fig. 8a shows the PAC spectra of a ^{111}Cd-implanted Ga_2O_3 bulk single-crystal after annealing in air at 1000 ºC, for two different orientations of the crystal with respect to the four gamma detectors.

A least square fit to the spectra (also shown in Fig. 8) reveals that the main component of the EFG is directed along the <201> axis of the Ga_2O_3 crystal with a magnitude of $V_{zz} = 6.0(1)\times10^{21}$ V/m^2 and η=0. Virtually all ^{111}Cd-probes are subjected to this EFG and therefore occupy the same lattice site. The low attenuation of the spectra, and the non-identification of other frequency triplets, further reveal the excellent recovery of the crystal structure, and the annihilation of point defects in the Cd neighborhood.

Fig. 8b reproduces previous PAC data taken on Ga_2O_3 NWs carried out under the same conditions as those used for the bulk crystal[19]. Directly after the implantation, the graph shows a strong attenuation of the PAC R(T) experimental function, typical for as-implanted samples due to the distribution of implantation defects around the probe. Still extra information is obtained from these spectra, i.e., the absence of additional well defined frequency triplets, as an evidence for extra EFGs, excludes the formation of priority specific defect configurations with the implanted dopant; i.e. all defects appear as being uncorrelated and not stabilized by the implanted impurity atom. After annealing at 800 ºC a clear pattern becomes visible corresponding to the same EFG as observed in the bulk crystals. However, only about 50% of the probe atoms are subjected to this EFG while the remaining probes reside in strongly disturbed lattice sites with a wide distribution of EFGs. This latter fraction of probes probably reside in regions of the crystal with a still large concentration of non-annealed implantation defects suggesting that higher annealing temperatures are necessary for a full recovery of the crystalline structure in agreement with the RBS data in section 3.1.

Ga-atoms occupy two distinct lattice sites in Ga_2O_3, the octahedral O_h and tetrahedral T_d sites[33]. Density functional theory calculations of the EFGs in Ga_2O_3 predict $V_{zz} = 6.02\times10^{21}$ V/m^2 for ^{111}Cd on the octahedral Ga-site and $V_{zz} = 4.67\times10^{21}$ V/m^2 for ^{111}Cd on the tetrahedral Ga-site[19]. The good agreement of the measured EFG with the calculations for the octahedral site suggests that ^{111}Cd is exclusively incorporated on the octahedral Ga-site in the Ga_2O_3 lattice, both in bulk crystals and NWs. In fact, this finding is in excellent agreement with theoretical ab initio calculations predicting the preferential incorporation of dopants into the octahedral Ga-site for a large number of divalent, trivalent and tetravalent dopants such as Mg, In, Cr, Si, Ge, Sn, and Zr.[34]

For the case of RE ions, the isovalency of the RE^{3+} defects with Ga and their large ionic radii also suggest the substitution of Ga on the octahedral site because of the larger nearest neighbor distance than for the tetrahedral site[19].

Downloaded From: http://proceedings.spiedigitallibrary.org/ on 03/09/2014 Terms of Use: http://spiedl.org/terms

Indeed, for Eu doped nanophosphors, optical spectroscopy data in combination with crystal field calculations suggested the incorporation of Eu in a single site, presumably the distorted octahedral Ga-site[6]. In fact, the non-degenerated character of $^5D_0 \rightarrow {}^7F_0$ transition, typically used to probe the Eu^{3+} crystallographic sites, suggests that Eu^{3+} ions should be placed in sites with lower symmetry than O_h or T_d. Furthermore, the asymmetric ratio between the $^5D_0 \rightarrow {}^7F_2$ and $^5D_0 \rightarrow {}^7F_1$ transitions hints to the lack of inversion symmetry on the site. PAC measurements with the RE probe ^{172}Lu are planned for the future to enlighten the lattice site of implanted RE ions in Ga_2O_3.

4. CONCLUSIONS

Ion implantation into Ga_2O_3 has been studied for bulk single crystals and NWs. The damage formation upon Eu implantation at RT and its recovery by RTA is found to be similar in both materials. In bulk crystals, amorphization starts at the surface at a fluence of $\sim 1\times10^{15}$ at/cm^2 and proceeds deeper into the crystal for the higher fluence of $\sim 4\times10^{15}$ at/cm^2. Similarly NWs are amorphized at this fluence. Defect recovery starts at annealing temperatures between 500 and 700 ºC, but close to complete recovery is only observed for RTA at ~1100 ºC in both bulk crystals and NWs. CL suggests that in both materials the same Eu^{3+} centers are optically active. PL on the other hand is only seen for the NW samples indicating that incorporation of Eu in optically active sites is more efficient. The absence of Eu^{3+} PL emission in bulk crystals is assumed to be related with the observed diffusion of Eu towards the surface and the fact that Eu is incorporated mainly on random lattice sites rather than substitutional Ga-sites where Eu could be expected to be in the optically active trivalent charge state. For low fluence ^{111}Cd implantation, the Ga_2O_3 lattice is completely recovered after annealing at 1000 ºC and all Cd-probes are substituting Ga on the octahedral site.

ACKNOWLEDGEMENTS

Financial support by FCT Portugal through grants PTDC/CTM-NAN/2156/2012, PTDC/FIS-NAN/0973/2012, CERN/FP/123585/2011, RECI/FIS-NAN/0183/2012 (FCOMP-01-0124-FEDER-027494), PEst-C/CTM/LA 25/2013, and individual grants "Investigador FCT" (KL), SFRH/ BD/76300/2011 (JR) is gratefully acknowledged. We thank R.A.S. Ferreira and V.P. Freitas (U. Aveiro) for their help in the PLE experiments. This work has been supported by MINECO through Projects MAT 2012-31959 and Consolider CSD 2009-00013.

REFERENCES

[1] Tippins, H.H., "Optical absorption and photoconductivity in the band edge of β-Ga_2O_3," Phys. Rev. A 140, 316-319 (1965).
[2] Ueda, N., Hosono, H., Waseda, R., and Kawazoe, H., "Synthesis and control of conductivity of ultraviolet transmitting β-Ga_2O_3 single crystals," Appl. Phys. Lett. 70, 3561 (1997).
[3] Feng, P., Xue, X. Y., Liu, Y. G., Wan, Q., and Wang, T. H., "Achieving fast oxygen response in individual β-Ga_2O_3 NWs by ultraviolet illumination," Appl. Phys. Lett. 89, 112114 (2006).
[4] Tokida, Y. and Adachi, S., "Photoluminescent Properties of Eu^{3+} in Ga_2O_3:Cr^{3+} Films Prepared by Metal Organic Deposition," Jap. J. Appl. Phys. 52, 101102 (2013) and references therein.
[5] Wellenius, P., Smith, E. R., LeBoeuf, S. M., Everitt, H. O., and Muth, J. F., "Optimal composition of europium gallium oxide thin films for device applications," J. Appl. Phys. 107, 103111 (2010).
[6] Zhu, H., Li, R., Luo, W., and Chen, X., "Eu^{3+}-doped β-Ga_2O_3 nanophosphors: annealing effect, electronic structure and optical spectroscopy," Phys. Chem. Chem. Phys. 13, 4411-4419 (2011).
[7] Nogales, E., Méndez, B., Piqueras, J., and García, J. A., "Europium doped gallium oxide nanostructures for room temperature luminescent photonic devices," Nanotechnology 20, 115201 (2009).
[8] Santos, N.F., Rodrigues, J., Fernandes, A.J.S., Alves, L.C., Alves, E., Costa, F.M., and Monteiro, T., "Optical properties of LFZ grown β-Ga_2O_3:Eu^{3+} fibres," Applied Surface Science 258, 9157– 9161 (2012).
[9] Alves, E., Lorenz, K., Vianden, R., Boemare, C., Soares, M. J., and Monteiro, T., "Optical doping of nitrides by ion implantation," Mod. Phys. Lett. B 15, 1281-1287 (2001).

Downloaded From: http://proceedings.spiedigitallibrary.org/ on 03/09/2014 Terms of Use: http://spiedl.org/terms

[10] Lorenz, K., Alves, E., Gloux, F., Ruterana, P., Peres, M., Neves, A. J., and Monteiro, T., "Optical doping and damage formation in AlN by Eu implantation," J. Appl. Phys. 107, 023525 (2010).
[11] Sasaki, K., Higashiwaki, M., Kuramata, A., Masui, T., and Yamakoshi, S., "Si-Ion Implantation Doping in β-Ga_2O_3 and its Application to Fabrication of Low-Resistance Ohmic Contacts," Appl. Phys. Express 6, 086502 (2013).
[12] Nogales, E., García, J.A., Méndez, B., Piqueras, J., Lorenz, K., and Alves, E., "Visible and infrared luminescence study of Er doped β-Ga_2O_3 and $Er_3Ga_5O_{12}$," Journal of Physics D: Applied Physics 41, 065406 (2008).
[13] Nogales, E., Hidalgo, P., Lorenz, K., Méndez, B., Piqueras, J., and Alves, E., "Cathodoluminescence of rare earth implanted Ga_2O_3 and GeO_2 nanostructures," Nanotechnology 22, 285706 (2011).
[14] López, I., Lorenz, K., Nogales, E., Méndez, B., Piqueras, J., Alves, E., and García, J. A., "Study of the relationship between crystal structure and luminescence in rare-earth-implanted Ga_2O_3 NWs during annealing treatments," J. Mater. Sci. 49, 1279–1285 (2014).
[15] Víllora, E.G., Shimamura, K., Yoshikawa, Y., Aoki, K., and Ichinose, N., "Large-size β-Ga_2O_3 single crystals and wafers," Journal of Crystal Growth 270, 420–426 (2004).
[16] Barradas, N. P., and Jeynes, C., "Advanced physics and algorithms in the IBA DataFurnace," Nucl. Instr. Meth. Phys. Res. B 266, 1875-1879 (2008).
[17] Wendler, E., Wesch, W., Götz, G., "Radiation damage and optical properties of Ar^+-implanted GaP," J. Appl. Phys. 70, 144 – 149 (1991).
[18] Bøgh, E., "Defect studies in crystals by means of channeling," Can. J. Phys. 46, 653 (1968).
[19] Barbosa, M.B., Gonçalves, J.N., Redondo-Cubero, A., Miranda, S.M.C., Simon, R., Kessler, P., Brandt, M., Henneberger, F., Nogales, E., Méndez, B., Johnston, K., Alves, E., Vianden, R., Araújo, J.P., Lorenz, K., Correia, J.G., "Nanostructures and thin films of transparent conductive oxides studied by perturbed angular correlations," Phys. Status Solidi B 250, 801–808 (2013).
[20] Lorenz, K., Peres, M., Franco, N., Marques, J. G., Miranda, S. M. C., Magalhães, S., Monteiro, T., Wesch, W., Alves, E., and Wendler, E., "Radiation damage formation and annealing in GaN and ZnO," Proc. of SPI 7940, 79400O (2011).
[21] Miranda, S. M. C., Peres, M., Monteiro, T., Alves, E., Sun, H. D., Geruschke, T., Vianden, R., and Lorenz, K., "Rapid Thermal Annealing of Rare Earth Implanted ZnO Epitaxial Layers," Optical Materials 33, 1139–1142 (2011).
[22] Wendler, E., Bilani, O., Gärtner, K., Wesch, W., Hayes, M., Auret, F.D., Lorenz, K., and Alves, E., "Radiation damage in ZnO ion implanted at 15 K," Nucl. Instr. Meth. Phys. Res. B 267, 2708–2711 (2009).
[23] Biersack, J.P., Ziegler, J.F., [The Stopping and Ranges of Ions in Matter], vol. 1, Pergamon Press, Oxford, (1985); SRIM2013 - http://www.srim.org/
[24] Kucheyev, S.O., Williams, J.S., Jagadish, C., Zou, J., Li, G., and Titov, A.I., "Effect of ion species on the accumulation of ion-beam damage in GaN," Phys. Rev. B 64, 035202 (2001).
[25] Lorenz, K., Wahl, U., Alves, E., Wojtowicz, T., Ruterana, P., Ruffenach, S., and Briot, O., "Amorphisation of GaN during processing with rare earth ion beams," Superlattices and Microstructures 36, 737-745 (2004).
[26] Wendler, E., Wesch, W., Azarov, A. Yu., Catarino, N., Redondo-Cubero, A., Alves, E., and Lorenz, K., "Comparison of low- and room-temperature damage formation in Ar ion implanted GaN and ZnO," Nucl. Instr. Meth. Phys. Res. B 307, 394–398 (2013).
[27] Götz, G., and Gärtner K. (eds.), [High Energy Ion Beam Analysis of Solids], Akademie-Verlag, Berlin, (1988).
[28] Shimamura, K., Víllora, E. G., Ujiie, T., and Aoki K., "Excitation and photoluminescence of pure and Si-doped β-Ga_2O_3 single crystals," Appl. Phys. Lett. 92, 201914 (2008).
[29] Wahl, U., Alves, E., Lorenz, K., Monteiro, T., Vantomme, A., de Vries, B., and Vianden, R., "Lattice location and optical activation of rare earth implanted GaN," Materials Science and Engineering B 105, 132-140 (2003).
[30] Segura-Ruiz, J., Martínez-Criado, G., Chu, M. H., Geburt, S., and Ronning, C., "Nano-X-ray Absorption Spectroscopy of Single Co-Implanted ZnO Nanowires," Nano Lett. 11, 5322–5326 (2011).
[31] Hauer, B., Vianden, R., Marques, J.G., Barradas, N.P., Correia, J.G., Melo, A.A., Soares, J.C., Agulló-Lopez, F., Dieguez, E., "Electric-field gradients at the ^{111}In and ^{111m}Cd sites in undoped and Mg-doped $LiNbO_3$," Phys. Rev. B 51, 6208-6214 (1995).
[32] Correia, J.G., Marques, J.G., Alves, E., Forkel-Wirth, D., Jahn, S.G., Restle, M., Dalmer, M., Hofsäss, H. and Baruth-Ram, K., "Microscopic studies of implanted ^{73}As in diamond," Nucl. Instrum. Meth B 127-128, 723-726 (1997).
[33] Geller, S., "Crystal Structure of β-Ga_2O_3,"J. Chem. Phys. 33, 676-684 (1960).
[34] Blanco, M.A., Sahariah, M.B., Jiang,H., Costales, A., and Pandey, R., "Energetics and migration of point defects in Ga_2O_3," Phys. Rev. B 72, 184103 (2005).

Downloaded From: http://proceedings.spiedigitallibrary.org/ on 03/09/2014 Terms of Use: http://spiedl.org/terms